Planetary Nebulae: A Universal Toolbox in the Era of Precision Astrophysics
Proceedings IAU Symposium No. 384, 2025
O. De Marco, A. Zijlstra & R. Szczerba, eds.
doi:10.1017/S1743921325001413

JWST imaging observations of the Ring Nebula

R. Wesson[1,2], Mikako Matsuura[1], Albert Zijlstra[3], Kevin Volk[4], Patrick J. Kavanagh[5,6], Guillermo García-Segura[7], I. McDonald[3,8], Raghvendra Sahai[9], M. J. Barlow[2], Nick L. J. Cox[10], Jeronimo Bernard-Salas[10,11], Isabel Aleman[12,13], Jan Cami[14,15,16], Nicholas Clark[14,15], Harriet L. Dinerstein[17], K. Justtanont[18], Kyle F. Kaplan[17], A. Manchado[19,20,21], Els Peeters[14,15,16], Griet C. Van de Steene[22] and Peter A. M. van Hoof[22]

[1]Cardiff Hub for Astrophysics Research and Technology (CHART), School of Physics and Astronomy, Cardiff University, The Parade, Cardiff CF24 3AA, UK

[2]Department of Physics and Astronomy, University College London, Gower Street, London WC1E 6BT, United Kingdom

[3]Jodrell Bank Centre for Astrophysics, Department of Physics & Astronomy, The University of Manchester, Oxford Road, Manchester M13 9PL, UK

[4]Space Telescope Science Institute, 3700 San Martin Drive, Baltimore, MD 21218, USA

[5]Department of Experimental Physics, Maynooth University, Maynooth, Co Kildare, Ireland

[6]School of Cosmic Physics, Dublin Institute for Advanced Studies, 31 Fitzwilliam Place, Dublin 2, Ireland

[7]Instituto de Astronomía, Universidad Nacional Autónoma de México, Ensenada, Mexico

[8]Department of Physical Sciences, The Open University, Walton Hall, Milton Keynes, MK7 6AA, UK

[9]Jet Propulsion Laboratory, California Institute of Technology, Pasadena, CA, USA

[10]ACRI-ST, Centred'Etudes et de Recherche de Grasse (CERGA), 10 Av. Nicolas Copernic, 06130 Grasse, France

[11]INCLASS Common Laboratory., 10 Av. Nicolas Copernic, 06130 Grasse, France

[12]Department of Computer Science, Institute of Mathematics and Statistics, University of São Paulo, Rua do Matão 1226, Cidade Universitária, 05508-090, São Paulo, SP, Brazil

[13]Instituto de Física e Química, Universidade Federal de Itajubá, Av. BPS 1303, Pinheirinho, 37500-903, Itajubá, MG, Brazil

[14]Department of Physics and Astronomy, University of Western Ontario, London, Ontario, Canada

[15]Institute for Earth and Space Exploration, University of Western Ontario, London, Ontario, Canada

[16]SETI Institute, Mountain View, CA, USA

[17]University of Texas at Austin, Austin, TX 78712, USA

[18]Chalmers University of Technology, Onsala Space Observatory, S-439 92 Onsala, Sweden

[19]Instituto de Astrofísica de Canarias, E-38205 La Laguna, Tenerife, Spain

[20]Departamento de Astrofísica, Universidad de La Laguna, E-38206 La Laguna, Tenerife, Spain

[21]Consejo Superior de Investigaciones Científicas (CSIC), Spain

[22]Royal Observatory of Belgium, Ringlaan 3, B-1180 Brussels, Belgium
email: rw@nebulousresearch.org

Abstract. We present *JWST* images of NGC 6720 (the Ring Nebula), covering wavelengths from 1.6 μm to 25 μm. The bright shell is strongly fragmented with some 20 000 dense globules, bright in H_2, with a characteristic diameter of 0.2 arcsec and density $n_H \sim 10^5$–10^6 cm^{-3}. The shell contains a narrow ring of polycyclic aromatic hydrocarbon (PAH) emission. H_2 is found throughout the shell and also in the halo. The central cavity is filled with high ionization gas and shows two linear structures seen in projection against the cavity. The central star is located 2 arcsec from the emission centroid of the cavity and shell. Linear features ('spikes') extend outward from the ring, pointing away from the central star. Around ten low-contrast, regularly spaced concentric arc-like features are present; they suggest orbital modulation by a low-mass companion with a period of about 280 yr. A previously known much wider companion is located at a projected separation of about 15 000 au; we show that it is an M2–M4 dwarf. NGC 6720 is therefore a triple star system. These features, including the multiplicity, are similar to those seen in the Southern Ring Nebula (NGC 3132) and may be a common aspect of such nebulae.

Keywords. stars: planetary nebulae; abundances dust; molecular abundances

1. Introduction

The Ring Nebula (NGC 6720 or M 57) is located at a distance of 790±30 pc, as derived from the *Gaia* parallax of the central star of 1.2696 ± 0.0438 mas (Lindegren et al. 2021). It has a visual diameter of about 4 arcmin (equivalent to $\sim 2 \times 10^5$ au or ∼1 pc) and shows a complex morphology (O'Dell et al. 2013). The distance puts the central star 190 pc above the Galactic plane, consistent with membership of the thin disk.

The central star currently has a temperature of $T_{\rm eff} = 1.35 \times 10^5$ K and a luminosity of $L \approx 310$ L$_\odot$ (Sahai et al, in prep.) which places it on the white dwarf cooling track. The current mass and progenitor mass of the central star are difficult to determine for objects on the cooling track, as the tracks tend to converge in that region of the HR diagram. González-Santamaría et al. (2021) quote 0.58 $M_\odot$ and 1.5 $M_\odot$, respectively, while the models of Miller Bertolami (2016) for the current temperature and luminosity are also consistent with a progenitor mass close to 2 $M_\odot$.

A post-AGB star of these masses reaches peak temperature at a luminosity $L \sim 3000\,L_\odot$. Fom this point, the luminosity declines to $\sim 200\,L_\odot$ within a few hundred years, before the decline slows down (Miller Bertolami 2016). The stellar luminosity of NGC 6720 ($L \approx 310\ L_\odot$) indicates that the star is currently in this phase of rapid fading. Part of the ionized nebula is likely recombining.

2. JWST Observations

The Ring Nebula was observed with *JWST* (Gardner et al. 2023) in Cycle 1 General Observers (GO) program 1558 (Figure 1). The observations were carried out in July and August 2022, using both NIRCam (Rieke et al. 2023) and MIRI (Wright et al. 2023).

The NIRCam observations were obtained on 2022 August 4th. Four filters were used, with two filters for each of the Short Wavelength Camera (F162M and F212N) and the Long Wavelength Camera (F300M and F335M). The nebula was covered by a single field of view (FOV) with a 4-point dither pattern yielding a FOV of 2.45 arcmin with some gaps near the edges of the fields which depend on the camera. The observing log is summarized in Table 1.

Imaging observations with MIRI were carried out on 2022 August 20th, using nine filters. The exposure time was 444 sec in each filter. The nebula was covered by a 1×2 mosaic with a 4-point dither pattern. The field size was 2.35×1.9 arcmin.

https://doi.org/10.1017/S1743921325001413 Published online by Cambridge University Press

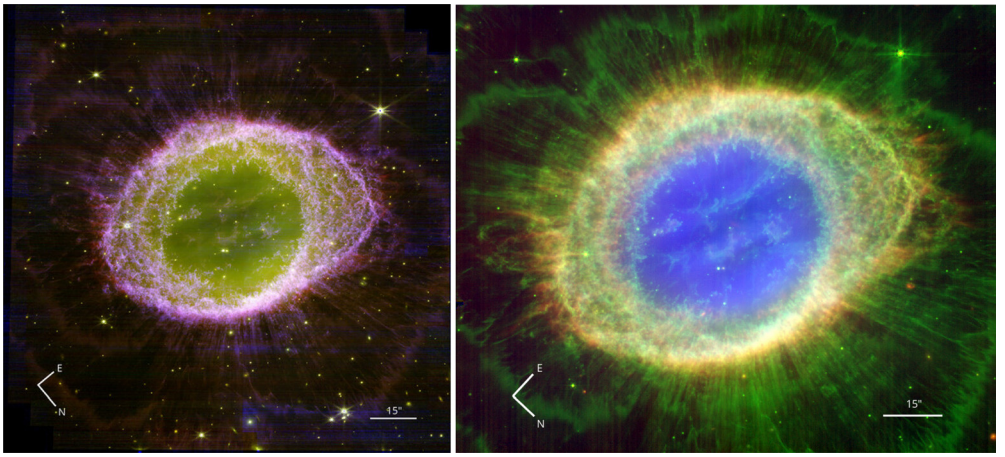

Figure 1. (l) NIRCam three colour image: F212N (blue), F300M (green) and F335M (red). (r) MIRI three-colour image: F2550W (blue), F560W (green) and F1130W (red). Directions of north and east are indicated.

Table 1. Observing log.

Instrument	Filter	λ_p (μm)	BW (μm)	PSF (")	t_{exp} (sec)	F_{tot} (Jy)	North Spec contributions Cont	H I	H_2	Others	Notes
NIRCam	F162M	1.626	0.168	0.053	1933	0.113±0.017	81%	10%	4%	He I (1%)	
	F212N	2.121	0.027	0.069	1933	0.9±0.08	13%		85%		
	F300M	2.996	0.318	0.097	483	0.1511±0.0002	58%	10%	27%	He II (1%)	
	F335M	3.365	0.347	0.109	483	0.2124±0.0003	53%	6%	37%		PAHs
MIRI	F560W	5.6	1.2	0.207	444	0.44±0.02	62%	2%	32%		
	F770W	7.7	2.2	0.269	444	0.816±0.01	68%	5%	14%	[Ar II] (9%)	PAHs
	F1000W	10.0	2.0	0.328	444	1.86±0.02	46%		11%	[S IV] (26%); [Ar III] (14%)	
	F1130W	11.3	0.7	0.375	444	0.7253±0.003	94%			[Ni I] (3%)	PAHs
	F1280W	12.8	2.4	0.420	444	1.20±0.02	45%	2%	1%	[Ne II] (49%)	
	F1500W	15.0	3.0	0.488	444	7.43±0.02	4%			[Ne III] (94%)	
	F1800W	18.0	3.0	0.591	444	4.01±0.02	42%			[S III] (54%)	
	F2100W	21.0	5.0	0.674	444	5.57±0.03	71%			[S III] (25%); [Ar III] (1%)	
	F2550W	25.5	4.0	0.803	444	20±2	88%			[O IV] (8%)	
MIRI Simul	F770W				951						
	F1130W				951						
	F1000W				951						

λ_p: pivot wavelength in μm (NIRCam: Rieke et al. 2023; MIRI: Bouchet et al. 2015). BW: band width in μm. PSF: FWHMs of PSFs in arcsec. For NIRCam simulated values are taken. t_{exp}: exposure time on source in sec. F_{tot}: photon-weighted mean flux density of the nebula in Jy. North Spec contributions: Estimated contributions to the images in each filter, calculated using NIRSpec-IFU and MIRI-MRS observations of a region in the northern part of the bright ring (van Hoof et al. in prep).

The pixel scales of the reduced data are 0.031 arcsec per pixel for the NIRCam short wavelength camera images, 0.063 arcsec for the NIRCam long wavelength camera images, and 0.111 arcsec for the MIRI images.

Table 1 lists the photon-weighted mean flux densities (F_{tot} in Jy) of the main body (the bright shell) of the Ring Nebula.

3. Nebular structure and stratification

The nebular images show three distinct regions: the central cavity, bright shell, and halo (Figure 2). The latter can be further divided into inner and outer halos. Multi-colour images reveal these components with different colours, indicating stratification

https://doi.org/10.1017/S1743921325001413 Published online by Cambridge University Press

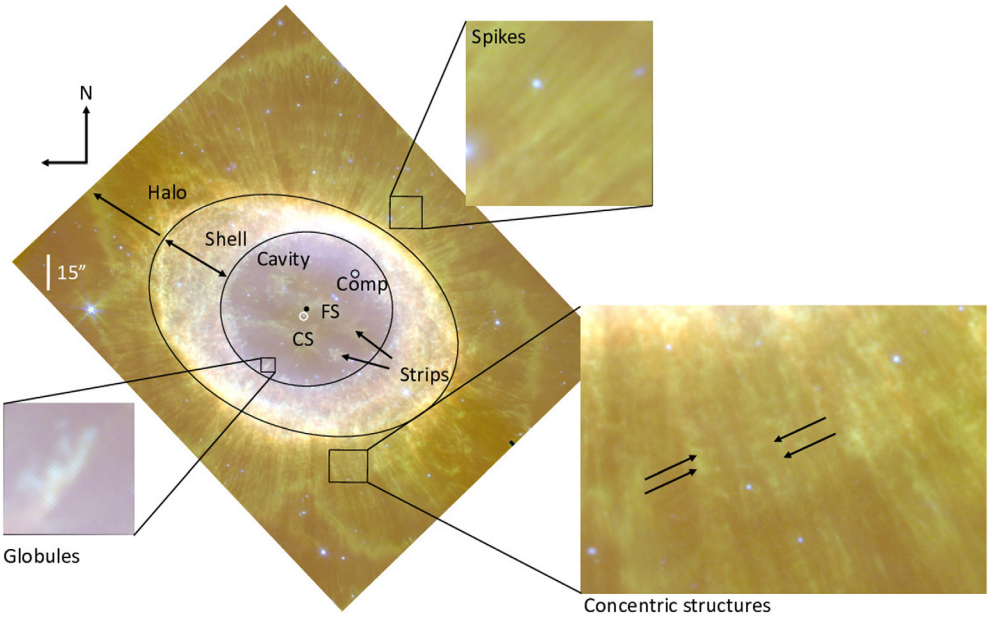

Figure 2. The names of the nebula components superposed on the NIRCam and MIRI three-colour image: F300M (blue), F560W (green) and F770W (red). CS (the white circle) is the central star, FS (black spot) is the first-moment centroid of the flux in the F300M image, and Comp is the companion star candidate. North is at the top in this image. The locations of some low-contrast concentric features are indicated, but they are much more easily seen in Fig. 3.

based on line emission. The low-density central cavity, emitting mainly in high-excitation [S IV] and [O IV] lines, has a circular outer edge. It contains a linear structure along its major axis, visible in various filters. The shell, surrounding the cavity, is an elliptical, clumpy region with a well-defined inner and outer edge. Its outer edge shows distortion, possibly related to the central star's proper motion. The inner halo, seen in various images, displays intricate structures including concentric arcs and radial spikes. The central star is detected in NIRCam and the two shortest-wavelength MIRI images.

Although the outer edge of the inner cavity is close to circular, its centre does not exactly correspond to the position of the central star, but instead appears to be offset to the north-west (roughly in the direction of the *Gaia* companion; see Sect. 3.5) by about 2 arcsec. The flux-weighted centres of the F300M and F335M images (calculated as the first moment of the images) are also offset from the central star, and nearly coincide with the centre of the inner cavity.

3.1. *Globules*

Even the angular resolution of the *JWST* images does not allow the system of globules to be cleanly resolved. To estimate their total number, we applied a peak-finding algorithm from the Python package PHOTUTILS (Bradley 2023) to the F212N image. The algorithm identifies about 17 500 peaks, which, given the density of clumps and resulting overlap, is likely to be an underestimate of the total number. A manual count was done in small regions, which, extrapolated to the full area, gives an estimated population of ∼25 000 globules.

The H_2 images reveal few cometary tails emanating from the globules. This is in contrast to the Helix Nebula where the majority of the globules (at least in the inner region)

https://doi.org/10.1017/S1743921325001413 Published online by Cambridge University Press

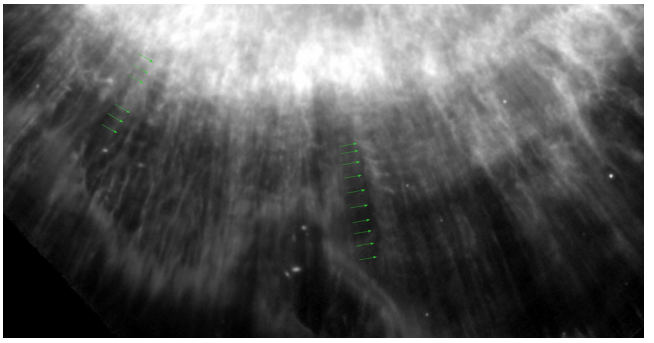

Figure 3. Regular concentric features in the outer regions of the F770W image of the Ring Nebula. Green arrows indicate the locations where these regularly-spaced features are most easily seen.

have well-developed tails seen in H_2 (Matsuura et al. 2009). Some short extensions of around 1 arcsec in length can be seen in absorption in the *HST* F502N and F658N images but these mostly do not have clear counterparts in the *JWST* images. The extensions seen in the *HST* images tend not to be straight. They may trace an early stage of tail formation.

3.2. *Radial spikes*

The halo shows multiple narrow, radial features pointing away from the central star, which following De Marco et al. (2022) we call 'spikes' (Fig. 3). They are seen only outside the bright shell, and mainly in H_2. The spikes are mainly a feature of the inner halo (O'Dell et al. 2013).

In a section of the F770W image covering 20 degrees of azimuth, we count 15–20 spikes. From this, we estimate that there are about 300–400 spikes in total. The exact number is imprecise due to the low contrast, small separation, and partial overlap of many spikes. The typical width appears to be around 0.4 arcsec. The typical length of the visible spikes is around 20 arcsec, but they may in a few cases extend twice as far, to the outer edge of the nebula.

The spikes are expected to arise from illumination effects where stellar light escapes through holes in the shell (De Marco et al. 2022). They line up better with the central star than with the offset centre of emission, which indicates that the dominant cause lies in the current or recent radiation from the star. There are some cases of misalignment with the star, possibly where there is partial overlap between spikes.

The number of spikes is of order 2 per cent of the number of globules. This suggests that there is no direct relation between the globules and spikes. O'Dell et al. (2013) argue that some of the spikes can be the shadows of large globules but this is not evident from the data here.

3.3. *Concentric arcs*

A series of faint, broken concentric arcs is apparent outside the bright ring in the H_2 halo. In places, up to 10 arcs can be identified (Figure 3). In some directions, the arcs appear to have been disrupted, possibly due to density variations in the nebula, but in general the curvature is regular.

The concentric structures are most apparent in the F770W image, which contains emission lines of H_2, H I and [Ar II]. They are also clearly visible in the F1000W and

https://doi.org/10.1017/S1743921325001413 Published online by Cambridge University Press

F1130W images and can be distinguished at longer wavelengths in the F1800W and F2100W filters, but at lower contrast due to the poorer spatial resolution. At shorter wavelengths with better spatial resolution, the much clumpier appearance of the nebula in the lines isolated by these filters makes the features harder to trace. The arcs are seen in most directions but are obscured by the shell along the major axis.

A common scenario invoked to explain arc systems like these is one in which a close binary companion modulates the outflow from the AGB star. The time interval of 280 years then corresponds to the orbital period of the companion. If the combined mass of the original AGB star and its companion is $1.5 \pm 0.5 M_{\odot}$, the orbital separation would be about 50 ± 15 au.

3.4. *PAHs*

The polycyclic aromatic hydrocarbon (PAH) feature at 11.3 μm has been detected in *Spitzer* spectra of the Ring Nebula (Cox et al. 2016) based on Program 40536 (P.I. H. Dinerstein). *Spitzer*'s Infrared Spectrograph (IRS) covered a 99×18 arcsec area along the major axis of the elliptically-shaped Ring Nebula, with a pixel scale of 1.8 arcsec. This spectral map showed that the PAH feature is emitted from the outer half of the shell, a more or less similar emitting region to the H_2 S(1) and S(2) lines at 17.04 and 12.28 μm.

The higher angular resolution *JWST* images allow the PAH-emitting regions to be studied in much more detail. The F335M filter encompasses the 3.3 μm PAH feature, while the F300M filter lacks this band but otherwise contains similar nebular emission (Table 1). The F1130W filter has the lowest contribution from emission lines (Table 1), and best reflects the contributions of the continuum and PAH bands. Both the F335M/F300M ratio image and the F1130W/F1000W ratio image show indications of a narrow ring of excess emission located at the outer edge of the shell.

This narrow ring shows up only in the two filters containing PAH bands and is not seen in other filter combinations. From Table 1, the PAH contribution to F335M and F1000W is < 14 per cent and < 7 per cent respectively, but this is estimated from MIRI IFU spectra which are not centred on the narrow ring. We interpret these narrow ring excesses as possible PAH emission.

3.5. *Multiplicity*

A distant companion to the central star was identified by González-Santamaría et al. (2021). This star, *Gaia* DR3 2090486687506009472, lies 18.5 arcsec from the central star, corresponding to a projected distance of 0.07 pc. González-Santamaría et al. (2021) proposed that this companion is a white dwarf, based on the *Gaia* DR3 photometry. However, the B_P and R_P photometry is discrepant from the G-band photometry by 2.74 mag, and appears to be significantly affected by nebular emission lines. We combined photometry from our NIRCam and MIRI observations as well as archival Hubble Space Telescope images to establish the properties of the companion star, using the Python Stellar Spectral Energy Distribution toolset (PySSED), an SED-fitting code based on the software presented in McDonald et al. (2009, 2012, 2017). We assume a distance to the star of 790 pc, and that the star has a composition of between $[Fe/H] = -0.4$ and $+0.0$ dex and a corresponding $[\alpha/Fe] = +0.1$ to $+0.0$ dex, based on its height of 190 pc from the Galactic plane. The Ring Nebula has a metallicity which is approximately solar (Liu et al. 2004; Guerrero et al. 1997). For a plausible range of values of extinction, the luminosity and temperature that we obtain correspond to a main sequence star of approximate spectral type M2–M4 with a mass of 0.3–0.5 $M_{\odot}$ (Cifuentes et al. 2020).

https://doi.org/10.1017/S1743921325001413 Published online by Cambridge University Press

4. Conclusion

JWST images have revealed a wealth of structural detail in NGC 6720. The nebula has a highly ionized inner cavity, a shell containing some 20 000 dense clumps, a thin ring of possible PAH emission, and a halo that contains around 10 concentric arcs and 400 spikes. Much of this detail is shown by the H_2 emission. The globules in the Ring Nebula have little or no tails, unlike those in the Helix Nebula. The globules in the Helix are also larger. These differences could be due to the Helix Nebula being more evolved and the Ring Nebula being in an earlier phase of evolution.

The central exciting star is inferred to be a member of a triple system. This consists of: the central star itself, with a progenitor mass of $\sim$1.5–2 $M_{\odot}$; a binary companion at some 50 au, responsible for the evenly spaced concentric arc structures in the nebula; and a distant, common proper motion companion at 0.07 pc which is a low-mass M2–M4 main sequence star.

Many features we see in the *JWST* images of the Ring Nebula, including the spikes, are shared by several other well-studied PNe of similar morphology. The time when planetary nebulae could be modelled as uniform density spheres is long gone. They contain a wide variety of structures and phases, with very different conditions and size scales, ranging from highly ionized hot gas to dense molecular clumps.

References

Bouchet P., et al., 2015, PASP, 127, 612
Bradley L., 2023, astropy/photutils: 1.8.0, doi:10.5281/zenodo.7946442
Cifuentes C., et al., 2020, A&A, 642, A115
Cox N. L. J., Pilleri P., Berné O., Cernicharo J., Joblin C., 2016, MNRAS, 456, L89
De Marco O., et al., 2022, Nature Astronomy, 6, 1421
Gardner J. P., Mather J. C., Abbott R., et al. 2023, arXiv e-prints, p. arXiv:2304.04869
González-Santamaría I., Manteiga M., Manchado A., Ulla A., Dafonte C., López Varela P., 2021, A&A, 656, A51
Guerrero M. A., Manchado A., Chu Y. H., 1997, ApJ, 487, 328
Lindegren L., et al., 2021, A&A, 649, A4
Liu Y., Liu X. W., Barlow M. J., Luo S. G., 2004, MNRAS, 353, 1251
Matsuura M., et al., 2009, ApJ, 700, 1067
McDonald I., van Loon J. T., Decin L., Boyer M. L., Dupree A. K., Evans A., Gehrz R. D., Woodward C. E., 2009, MNRAS, 394, 831
McDonald I., Zijlstra A. A., Boyer M. L., 2012, MNRAS, 427, 343
McDonald I., Zijlstra A. A., Watson R. A., 2017, MNRAS, 471, 770
Miller Bertolami M. M., 2016, A&A, 588, A25
O'Dell C. R., Ferland G. J., Henney W. J., Peimbert M., 2013, AJ, 145, 92
Rieke M. J., Kelly D. M., Misselt K., et al. 2023, PASP, 135, 028001
Wright G. S., Rieke G. H., Glasse A., et al. 2023, PASP, 135, 048003

https://doi.org/10.1017/S1743921325001413 Published online by Cambridge University Press